Calculation of Polarization Using a Density Functional Method with Localized Charge

L. L. Boyer,[1] H. T. Stokes,[2] and M. J. Mehl[1]

[1]*Center for Computational Materials Science, Naval Research Laboratory, Washington, D.C. 20375-5345*

[2]*Department of Physics and Astronomy, Brigham Young University, Provo, Utah 84602*

(Received 28 January 1999)

A density functional method, which represents the total charge density as a sum of self-consistently determined localized densities, is described. While this approach is generally less accurate than conventional band-structure methods, it offers a relatively simple interpretation of polarization and related properties. The method is illustrated with results for NaCl, MgO, and AlP.

PACS numbers: 71.15.Mb, 63.20.Dj, 77.22.Ej

The most common applications of density functional theory (DFT) follow the Kohn-Sham (KS) method [1], in which the density is expressed in terms of Bloch functions. The delocalized nature of these functions make the computation of polarization, or rather changes in polarization, a nontrivial matter, which, only recently, has been resolved [2,3]. On the other hand, if the charge density can be represented as a sum over localized densities, then changes in polarization are given directly by changes in the dipole moment of the crystallographic unit cell. In this Letter we demonstrate that the latter picture also can be applied within DFT by a method we call self-consistent atomic deformation (SCAD). In addition to simplified expressions for polarization, SCAD offers an efficient $O(N)$ (order N) method for treating large systems. That is, the computational requirements of the SCAD method increase in proportion to the number of atoms in the unit cell.

In the SCAD method the electronic density is given by

$$n(\mathbf{r}) = \sum_i n_i(\mathbf{r} - \mathbf{R}_i), \tag{1}$$

where the n_i are localized and expanded in terms of spherical harmonics about the sites of the atomic nuclei,

$$n_i(\mathbf{r}) = \sum_{l,m} n_{lm}^{(i)}(r) Y_{lm}(\hat{\mathbf{r}}). \tag{2}$$

Each atomiclike density n_i is determined from the solutions of a one-electron Schrödinger's equation with a similarly expressed potential

$$v_i(\mathbf{r}) = \sum_{l,m} v_{lm}^{(i)}(r) Y_{lm}(\hat{\mathbf{r}}), \tag{3}$$

formulated variationally from the total energy [4]:

$$E[n] = \sum_i (T_0[n_i] - T_k[n_i]) + T_k[n] + F[n]; \tag{4}$$

$$v_i(\mathbf{r}) = v_F[n(\mathbf{r})] + v_k[n(\mathbf{r})] - v_k[n_i(\mathbf{r})]. \tag{5}$$

In the above expressions $T_0[n_i]$ is the kinetic energy of noninteracting electrons centered about the site at $\mathbf{R}_i$, T_k is a functional to account for the kinetic energy due to overlapping densities [the Thomas-Fermi (TF) expression is used here], F denotes all nonkinetic (exchange-correlation [5] and electrostatic) contributions to the total energy and v_F (v_k) are the functional derivatives of F (T_k).

The one-electron Schrödinger's equations are solved using basis functions with Slater-type radial dependence as listed in the tables of Clementi and Roetti [6]. Angular dependence is obtained by multiplying the radial functions by spherical harmonics (Y_{lm}) with $l_r \le l \le l_{\max}$ where l_r identifies the radial function. The self-consistent solution for v_i (and hence, n_i and n), obtained by occupying the lowest one-electron energy levels for the entire system, allowing for charge transfer when indicated, minimizes the total energy in accord with Janak's theorem [7]. This aspect of SCAD is the same as the KS formulation of DFT. It can also be considered an extension of the Gordon-Kim [8] method. In fact, some of the earliest density functional formulations of total energy were done in terms of overlapping atomic densities [9].

Expressing the total density as a sum over localized densities is not a fundamental approximation, since any density can be represented by Eq. (2). The Hohenberg-Kohn theorem [10] ensures that the *total* density will be given correctly, to the extent that the approximate total-energy functional is adequate. If an adequate representation of the total density is expressed in terms of localized densities, then changes in polarization, due to external fields or structural distortions, are determined straightforwardly by accounting for changes in dipole moments of the localized densities. This is true provided there is no charge transfer from one ion to another, which is the prevailing condition in the SCAD model for nonmetallic systems. The compounds treated here have their highest occupied levels (negative-ion p states) filled with six electrons. Directional bonding is achieved by distortion of the negative-ion density from spherical.

The numerical methods involved in implementing SCAD have been discussed briefly in previous publications [11,12], a detailed discussion of the method for spherically symmetric ions is available [13], and a more comprehensive paper on the general SCAD method is in preparation [14]. Two SCAD computer codes were developed, largely independently, at BYU and NRL. Detailed comparisons of results from the two codes

were instrumental in resolving problems and improving numerical methods. In general, errors resulting from the kinetic energy overlap term can be significant [12]. The lattice parameter for compounds that have overlapping p-like and d-like densities, e.g., AgCl or GaP, tend to be too large by $\sim$10%. However, as we shall see, the TF approximation does reasonably well for the compounds selected in this study.

For the calculations reported here, we use $l_{\max} = 2$ for the positive-ion p states and $l_{\max} = 3$ for the negative-ion p states of Cl^{-1} and O^{-2}. Inclusion of higher l spherical harmonics in the bases for NaCl and MgO was tested and found to be unimportant. We find that including the $l = 4$ spherical harmonics in the basis for the p states of phosphorus produces some change in the results for AlP. For example, going from $l_{\max} = 3$ to $l_{\max} = 4$ produces an 0.8% increase in the lattice parameter. Higher l values were not tested because our code is currently limited to $l_{\max} = 4$.

Calculation of the potential and total energy involves the definition of a "cutoff" radius, R_c. This serves two functions: (1) short-range contributions from overlapping densities are excluded for atoms with separations larger than R_c; and (2) electrostatic interactions for separations less than R_c are included "exactly," while such interactions for neighbors with separations greater than R_c are included as point poles (monopoles, dipoles, and quadrupoles). The present versions of our SCAD programs use the Ewald technique for including the long-ranged interactions. Strictly speaking, this makes the computation time scale as $O(N^2)$ for large N. Efficient fast multipole algorithms with $O(N \log N)$ or $O(N)$ scaling are available [15], which could be installed to handle long-ranged interactions for large N. We estimate that $N \sim 300$ would result in about half the total time devoted to the Ewald computations.

As long as one is interested in energy changes for small distortions of a given structure, such as those needed to compute lattice parameters, bulk moduli, and phonon frequencies, then a value of R_c which includes $\sim$30 neighbors may be sufficient. However, if accurate energies associated with large distortions are required, as in the comparison of the energies of two crystal structures, then a larger R_c, including up to $\sim$90 neighbors, may be needed. For example, the minimum energy for AlP in the B3 (zinc blende) structure is found to be lower than that in the B1 (rock salt) by $\sim$1.5 eV using large R_c (converged) results. However, if we choose R_c to contain 28 (26) neighbors in the B3 (B1) structures then the energy difference is only $\sim$0.03 eV. At the same time, using the smaller R_c changes the lattice parameter by less than 1% and the bulk modulus by only a few percent.

The remaining results reported here were obtained using the 56 (46) neighbor SCAD model for the B1 (B3) structures. Values for the lattice constants and bulk moduli are listed in Table I. The overall comparison with experiment is reasonably good, especially considering that the experimental values are for room temperature. However, for AlP the lattice constant is $\sim$4% too small, and this error contributes to a substantial overestimate of the bulk modulus.

TABLE I. Comparison of SCAD-model results with experimental values [16] for lattice parameters a (Bohr), bulk moduli B (10^{12} dyn/cm^2), dielectric constant ϵ_∞, Born effective charges Z^*, and the optic mode frequencies ν_{LO} and ν_{TO} (cm^{-1}).

	NaCl		MgO		A1P	
Property	SCAD	Expt.	SCAD	Expt.	SCAD	Expt.
a	10.54	10.66	7.91	7.97	9.91	10.33
B	0.254	0.240	1.81	1.64	1.47	0.86
ϵ_∞	2.26	2.35	2.86	3.01	6.56	7.54
Z^*	1.15	1.11	2.21	1.98	2.93	2.31
ν_{LO}	160	162	358	396	440	422
	270	259	777	712	564	504

We have computed the high frequency dielectric constant, ϵ_∞, for SCAD-modeled crystals with and without surfaces. While our codes assume periodic boundary conditions, we are able to model crystals with surfaces by creating a periodic array of slabs. This procedure was tested by varying the width of the slabs and the space between them.

Consider the application of an external electric field with strength E_z in the z direction to a crystal with finite size in the z direction. This requires the addition of terms $R_z^{(i)} E_z \sqrt{4\pi}$ to $v_{0,0}^{(i)}(r)$ and $E_z r \sqrt{4\pi/3}$ to $v_{1,0}^{(i)}(r)$, where $R_z^{(i)}$ is the z component of $\mathbf{R}_i$. However, if the crystal is infinite in all directions, periodic boundary conditions remove the $l = 0$ contribution. In either case, the external field produces dipole ($l = 1$) contributions to the densities. For the infinite crystal, polarization ($\mathbf{P}$) produced by the electric field is determined simply by adding the dipole moments induced on each ion in the unit cell and dividing by the volume per unit cell. In this case the total macroscopic electric field is just the external field, and the third (z) column of the dielectric tensor is $4\pi P_x/E_z$, $4\pi P_y/E_z$, and $1 + 4\pi P_z/E_z$. Of course, the dielectric tensors for the cubic-symmetry compounds treated here are diagonal with equal elements (ϵ_∞) on the diagonal.

In the slab simulation, polarization is determined from dipole moments of ions far enough from the surface to give a position independent result for $\mathbf{P}$. Then, to obtain the dielectric constant from the polarization, we need to use the *total* macroscopic electric field in the bulk. For the slab geometry, the moments induced by the external field can themselves produce a macroscopic electric field in the z direction. We determine this induced macroscopic field from the variation of the electrostatic potential at the nucleus of each ion in the bulk, due to all the *other* ions, as a function of the ion's position. The induced field, computed in this way, is independent of position as long as the periodic slabs are sufficiently thick and far enough apart. We have tested this with calculations for MgO and find

that the dielectric constant obtained this way agrees precisely with that determined by the simpler method which exploits periodic boundary conditions. Values of ϵ_∞ for NaCl, MgO, and AlP are listed in Table I for comparison with experiment. The agreement is reasonably good, with the SCAD values consistently too small. We note that the KS method overestimates ϵ_∞ by a similar amount [17].

The values of ϵ_∞ and Z^*, the Born effective charge, determine the splitting of the longitudinal and transverse optic (LO and TO) modes. Specifically, the dynamical matrix has a term that depends on the *direction* of the wave vector [18]. In our case the LO mode frequency becomes

$$\nu_{\mathrm{LO}}^2 = \nu_{\mathrm{TO}}^2 + \frac{4\pi e^2 (Z^*)^2}{V \epsilon_\infty \mu}, \qquad (6)$$

where e is the electronic charge, V is the volume per primitive cell, and μ is the reduced mass. Computation of Z^* is straightforward using SCAD [11]. We simply displace an ion a small amount and determine the induced dipole moments on all the ions in the unit cell. The induced moments together with the moment due to the displacement give the net change in polarization, which in turn defines Z^*. Results for Z^* of the positive ions of NaCl, MgO, and AlP are listed in Table I. (Values for the negative ions are, of course, the negative of those for the positive ions.) We use the frozen-mode method [19] to compute the TO mode frequency and Eq. (6) to get the LO mode frequency. The LO and TO mode frequencies are also listed in Table I. While the agreement with experimental values is reasonably good, the SCAD values for the LO-TO splitting are consistently too large, owing to ϵ_∞ values that are too small and Z^* values that are too large.

Finally, we have carried out frozen-mode calculations for wave vectors at the fractions $1/4$, $1/2$, $3/4$, and 1 of the way from Γ to X in the Brillouin zone. The modes at X require a 4-ion supercell, modes at $X/2$, an 8-ion supercell, and modes at $X/4$ and $3X/4$, a 16-ion supercell. If our calculations for Z^* and ϵ_∞ are carried out correctly, then the value determined for ν_{LO} should join smoothly with the frequencies along the LO branch from Γ to X. These results are displayed in Figs. 1, 2, and 3. In these plots, lines for the optical branches are determined by a Fourier expansion that exactly fits the five frequencies determined from Γ to X. The lines presented for the acoustic modes are determined by a lower order, least squares fit, since the errors from the frozen-mode method are generally more pronounced for the lower frequency modes. The LO mode frequencies at Γ do appear to join smoothly with the rest of the frequencies on the LO branches.

In conclusion, we have described calculations of polarization and related properties for NaCl, MgO, and AlP using a density functional method in which the total density is expressed as a sum of self-consistently determined localized densities. Based on the comparison of our results

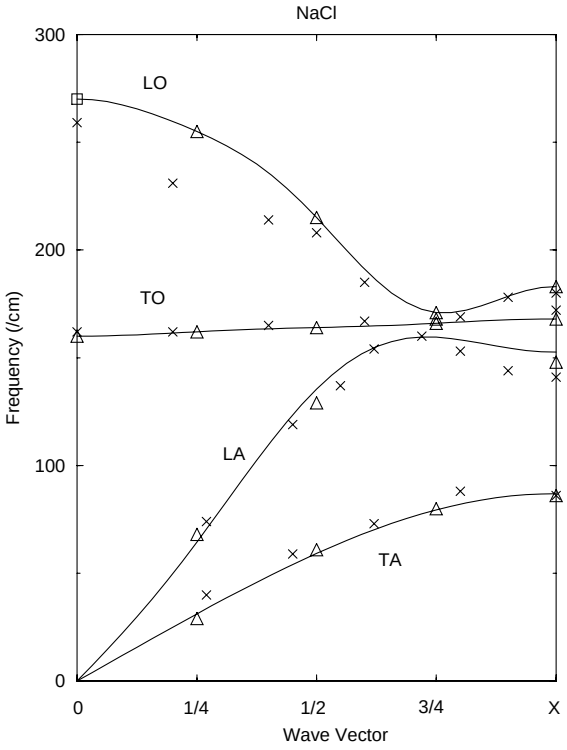

FIG. 1. Dispersion curves in the Δ direction for NaCl, based on frequencies determined from SCAD frozen-mode energies ($\triangle$) and Eq. (6) ($\square$) for comparison with experimental values [16] ($\times$).

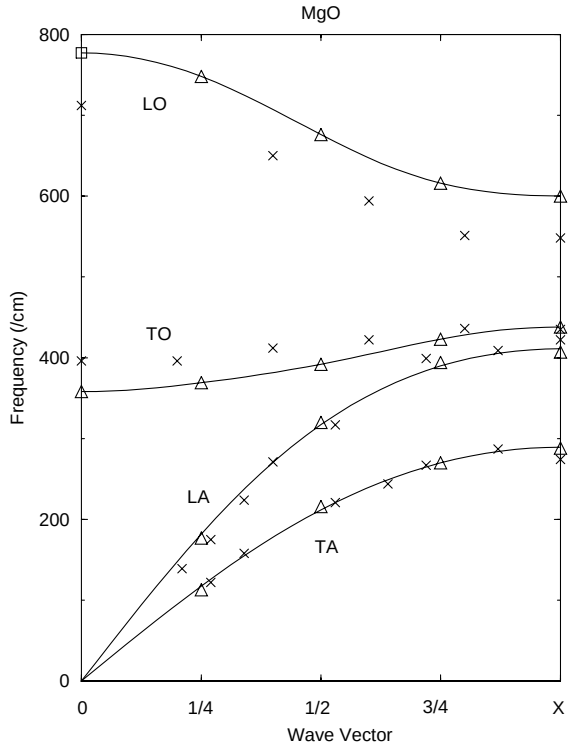

FIG. 2. Dispersion curves in the Δ direction for MgO, based on frequencies determined from SCAD frozen-mode energies ($\triangle$) and Eq. (6) ($\square$) for comparison with experimental values [16] ($\times$).

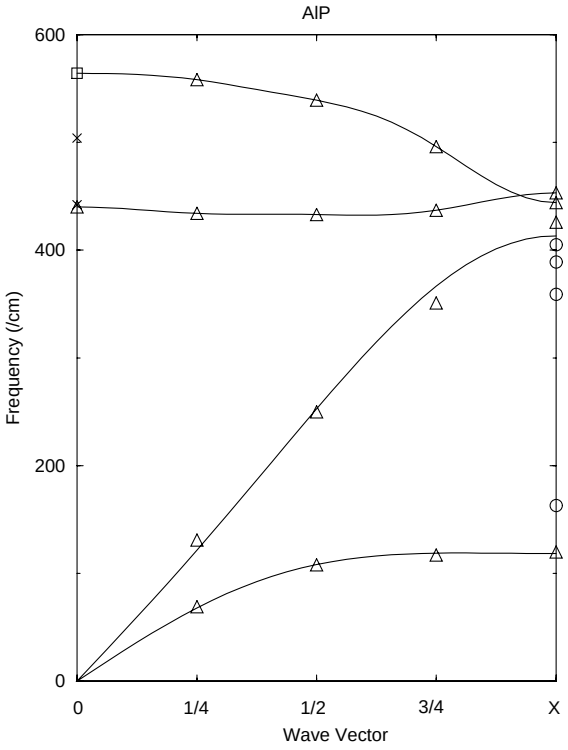

FIG. 3. Dispersion curves in the Δ direction for AlP, based on frequencies determined from SCAD frozen-mode energies ($\triangle$) and Eq. (6) ($\square$) for comparison with experimental values [16] ($\times$) and from other DFT calculations [20] ($\circ$).

to experimental quantities, the internal consistency of our results for crystals with and without surfaces, and the fact that our computed values for ν_{LO} join smoothly with the other modes on the LO branch, we believe our basic approach for computing polarization and related properties is valid. It is evidently applicable to a wider range of problems than would be expected from presentation [3] of the band-structure approach.

This work was supported by the Office of Naval Research.

[1] W. Kohn and L. J. Sham, Phys. Rev. **140**, A1133 (1965).
[2] R. D. King-Smith and D. Vanderbilt, Phys. Rev. B **47**, 1651 (1993).
[3] R. Resta, Rev. Mod. Phys. **66**, 899 (1994).
[4] M. J. Mehl, L. L. Boyer, and H. T. Stokes, J. Phys. Chem. Solids **57**, 1405 (1996).
[5] L. Hedin and B. I. Lundqvist, J. Phys. C **4**, 2064 (1971).
[6] E. Clementi and C. Roetti, At. Data Nucl. Data Tables **14**, 177 (1974).
[7] J. F. Janak, Phys. Rev. B **18**, 7165 (1978).
[8] R. G. Gordon and Y. S. Kim, J. Chem. Phys. **56**, 3122 (1972).
[9] M. Born and K. Huang, *Dynamical Theory of Crystal Lattices* (Oxford Press, London, 1954), Chap. 1, and references therein.
[10] P. Hohenberg and W. Kohn, Phys. Rev. **136**, B864 (1964).
[11] L. L. Boyer, H. T. Stokes, and M. J. Mehl, Ferroelectrics **194**, 173 (1997).
[12] L. L. Boyer, H. T. Stokes, and M. J. Mehl, in *First Principles Calculations for Ferroelectrics*, edited by R. E. Cohen, AIP Conf. Proc. No. 436 (AIP, New York, 1998), p. 227.
[13] H. T. Stokes, L. L. Boyer, and M. J. Mehl, Phys. Rev. B **54**, 7729 (1996).
[14] L. L. Boyer, H. T. Stokes, and M. J. Mehl (to be published).
[15] M. Challacombe, C. White, and M. Head-Gordon, J. Chem. Phys. **107**, 10 113 (1997), and references therein.
[16] Experimental values correspond to room temperature and were collected from the following: M. P. Tosi, Solid State Phys. **16**, 1 (1964) (*a* and *B*); R. P. Lowndes and D. H. Martin, Proc. R. Soc. London Sect. A **308**, 473 (1969) (ϵ_∞); R. E. Schmunk and D. R. Winder, J. Phys. Chem. Solids **31**, 131 (1970) (frequencies), for NaCl; in *Numerical Data and Functional Relationships in Science and Technology,* Landolt-Bornstein, New Series, edited by O. Madelung (Springer-Verlag, Berlin, 1982), Vols. 17a and 17b for MgO and AlP; and M. J. L. Sangster, G. Peckham, and D. H. Saunderson, J. Phys. C **3**, 1026 (1970) (MgO dispersion curves).
[17] S. de Gironcoli, S. Baroni, and R. Resta, Phys. Rev. Lett. **62**, 2853 (1989).
[18] R. M. Pick, M. H. Cohen, and R. M. Martin, Phys. Rev. B **1**, 910 (1970).
[19] Symmetry constraints of the frozen-mode method are imposed using the compilation: H. T. Stokes and D. M. Hatch, *Isotropy Subgroups of the 230 Crystallographic Space Groups* (World Scientific, Singapore, 1988).
[20] C. O. Rodriguez, R. A. Casali, E. L. Peltzer, O. M. Cappannini, and M. Methfessel, Phys. Rev. B **40**, 3975 (1989).